

## FINITE ELEMENT MODIFIED METHOD OF CHARACTERISTICS FOR ION/PARTICLE TRANSPORT IN AN IMS MICRO-CHAMBER

Leo Gonzalez<sup>a</sup> and Alejandro Allievi<sup>b</sup>

<sup>a</sup>*Universidad Politécnica de Madrid, Canal de Ensayos Hidrodinámicos, Escuela Técnica Superior de Ingenieros Navales, Avda. Arco de la Victoria s/n - 28040 Madrid, Spain, leo.gonzalez@upm.es, <http://canal.etsin.upm.es/>*

<sup>b</sup>*Laboratorio de Micro y Nanomecánica, Instituto Tecnológico de Buenos Aires, Av. Eduardo Madero 399 (C1106ACD), Buenos Aires, Argentina, Alejandro.Allievi@gmail.com, aallievi@itba.edu.ar, [http://www.itba.edu.ar/lab\\_micro\\_y\\_nanomecanica/](http://www.itba.edu.ar/lab_micro_y_nanomecanica/)*

**Keywords:** Finite element, characteristics, microfluidics, ion/particle transport, IMS.

**Abstract.** We consider advection of a cluster of ions/particles along a backward-facing-step-like geometry that mimics the longitudinal mid-section of the microscale chamber of an Ion Mobility Spectrometer (IMS). In order to study the cluster's transport along the IMS chamber, we implement a Finite Element algorithm for the solution of the incompressible Navier-Stokes equations based on the Modified Method of Characteristics. The scheme combines a Lagrangian approach given by the Modified Method of Characteristics, which transforms the time dependent Navier-Stokes problem at every time step into a stationary Stokes problem, and an Eulerian perspective, which solves the Stokes problem by a Conjugate Gradient Algorithm (CGA). The Navier-Stokes equations are solved in the laminar regime using a mesh composed of Taylor-Hood triangular elements. The detection electrodes are simulated by means of outflow boundary conditions that provide estimates of the energy necessary to attract the cluster. Ions/particles trajectories are monitored to study their mobility within the flow and to optimize the electrodes' location.

## 1 INTRODUCTION

Ion Mobility Spectrometry (IMS) is an analytical approach that encompasses theories, methodologies, and devices used to characterize chemical substances on the basis of the velocity of gas-phase ions in an electric field (Iceman and Karpas, 1993, 2005). Typical applications are detection of toxic industrial products, chemical warfare agents, explosives and explosives-related compounds, and narcotics. IMS' several advantages include high resolution (ppb), very fast measurements (msec), operation at atmospheric conditions, lighter equipment, reliability and relatively low cost of operation.

IMS relies on a relatively simple working principle: the time-of-flight of a cluster of ions along a chamber, also known as the drift tube, that contains ionization and detection regions, Figure 1 (Ortiz et al., 2009). In traditional designs, the cluster of ions (normally generated by radioactive sources, photo-discharge lamps, lasers, electrospray ion sources, flames, corona discharges, or surface ionization sources) is convected along a *uniform-cross-section* chamber by an electric field. The field causes the separation of ions from different chemical substances, and these can be identified by their mobility spectrum generated by the arrival time at the detection region of the device, Figure 2. Traditional designs require chambers/drift tube lengths in the order of tens of centimeters. In addition, most drift tubes are generally constructed by a series of conducting drift rings separated by electric insulators (Ewing et al., 2001), which make their construction expensive. In order to reduce costs and overall dimensions to hand-held proportions, the last decade has seen the proliferation of smaller devices made by microfabrication techniques (Xu et al., 2000; Miller et al., 2000, 2001; Teepe et al., 2001; Guevremont and Kolakowski, 2005; Owlstone Nanotech Inc., 2006; Kalms et al., 2007; Zimmermann and Barth, 2007; Cumeras et al., 2009, 2010, 2011).

As pointed out in (Cumeras et al., 2011), research in microscale IMS devices has focused on a technology known as FAIMS (high-Field Asymmetric waveform Ion Mobility Spectrometry). In FAIMS, ions are convected along a *uniform* rectangular-cross-section drift tube by a co-flowing carrier gas. Conveniently located planar parallel electrodes provide an alternating time-varying high electric field  $E(t)$  oriented at  $90^\circ$  to the gas flow, causing the ions to follow trajectories normal to the flow. In contrast to low  $E$ -fields where mobilities  $K$  of ions are essentially constant, under high  $E(t)$  they become field dependent, i.e.,  $v_\perp = K(E)E(t)$ . As a result, improved separation and selection has been reported (Buryakov et al., 1993; Guevremont and Purves, 1999; Miller et al., 2000; Guevremont, 2004).

In this work, we report work in progress of flow in a backward-facing-step geometry to simulate a *non-uniform* IMS drift tube. We study the convection of a cluster of ions/particles that are released at the inlet of the drift chamber. To mimic the detection electrodes, we introduce outflow boundary conditions that attract the cluster.

The remaining of the paper is organized as follows. Section 2 describes the governing equations of the problem, namely the Navier-Stokes equations and the boundary conditions. Section 3 introduces the semi-discrete characteristics algorithm used to solve the Navier-Stokes problem and directs the reader to further details published elsewhere. In Section 4, we introduce geometric details and the method used to track the cluster of ions/particles. Section 5 presents our results, and Conclusions are stated in Section 6.

## 2 STATEMENT OF THE PROBLEM

Let  $\Omega \subset \mathbf{R}^d$  ( $d = 2$ ) be an open bounded domain with boundary  $\Gamma$  sufficiently smooth. We shall assume that  $\Gamma = \Gamma_1 \cup \Gamma_2$ , with the two subsets  $\Gamma_1$  and  $\Gamma_2$  satisfying  $\Gamma_1 \cap \Gamma_2 = \emptyset$ . The

Navier-Stokes equations describing unsteady flow of an incompressible Newtonian fluid are:

$$\frac{D\mathbf{u}}{Dt} - \nu\Delta\mathbf{u} + \nabla p = \mathbf{f} \quad \text{in } \Omega \times (0, T) \quad (1)$$

$$\nabla \cdot \mathbf{u} = 0 \quad \text{in } \Omega \times [0, T) \quad (2)$$

These equations are solved subject to the initial and boundary conditions

$$\mathbf{u}(\mathbf{x}, 0) = \mathbf{u}_0(x) \quad \text{in } \Omega \quad (3)$$

$$\mathbf{u}(\mathbf{x}, t) = \mathbf{g}_1(x, t) \quad \text{on } \Gamma_1 \quad (4)$$

$$-p\mathbf{n} + \nu\frac{\partial\mathbf{u}}{\partial\mathbf{n}} = \mathbf{g}_2(x, t) \quad \text{on } \Gamma_2 \quad (5)$$

where  $\mathbf{n}$  is the outward unit normal to the boundary  $\Gamma$ . Hereafter, vector fields shall be denoted by boldface letters and generic points of  $\bar{\Omega} = \Omega \cup \Gamma$  as  $x = (x_1, \dots, x_d)$ . The notation used in (1) – (2) is the following:

i)  $\mathbf{u} = (u_i)_{i=1}^d$  is the velocity,  $p$  is the pressure and  $\nu$  is the kinematic viscosity coefficient.

ii)  $\frac{D\mathbf{u}}{Dt} = \frac{\partial\mathbf{u}}{\partial t} + \mathbf{u} \cdot \nabla\mathbf{u}$  denotes the material derivative of  $\mathbf{u}$ . It measures the rate of change of  $\mathbf{u}$  along the trajectories of the fluid particles as seen by an observer moving with the flow.

iii)  $\mathbf{f} = (f_i)_{i=1}^d$  is a density of external forces.

Notice that (5) is a condition of the traction vector  $\mathbf{t} = -p\mathbf{n} + \nu\frac{\partial\mathbf{u}}{\partial\mathbf{n}}$ . As discussed by Gresho (Gresho, 1991), it may result in a better characterization of the outflow boundary condition. This enforces explicitly a zero variation in the normal direction to the boundary in contrast to the corresponding boundary condition on the stress tensor.

The existence and possible uniqueness of the solution to the system (1) – (5) have been studied in a number of books and papers by, among others, Temam (Ladyzhenskaya, 1969; Heywood, 1980; Temam, 1985). Computing its numerical solution is not trivial for the following reasons:

- 1) The equations are nonlinear.
- 2) The incompressibility condition (2).
- 3) The coupling of the equations through the terms  $\mathbf{u} \cdot \nabla\mathbf{u}$  and  $\nabla \cdot \mathbf{u}$ .

In order to overcome some of these difficulties, in the following section we summarize the implementation of a finite element-modified method of characteristics scheme. As we shall see below, this scheme belongs to the category of methods of fractional steps. The first stage of our method is a Lagrangian step followed by an Eulerian procedure where a Stokes problem is solved.

### 3 THE SEMIDISCRETE CHARACTERISTICS ALGORITHM

Due to the well known advantages of the semi-Lagrangian schemes when applied to advection dominated flows, see (Staniforth and Cote, 1981; Smolarkiewicz and Pudykiewicz, 1992; Strain, 1999) and references therein, we propose such a scheme for the treatment of the material derivative  $D/Dt$  in the Navier-Stokes equations, combined with mixed Taylor-hood finite elements for the spatial discretization.

Let the time interval  $[0, T]$  be divided into  $N$  intervals  $[t_n, t_{n+1}]$  of length  $\Delta t$  such that  $N\Delta t = T$ . For each interval  $[t_n, t_{n+1}]$  we integrate equations (1) – (5) along the trajectories of the fluid particles as described in the following developments. We introduce the notation  $X(x, t_{n+1}; t)$  to denote the position at time  $t$  of a fluid particle that reaches the point  $x \in \bar{\Omega}$  at time  $t_{n+1}$ . The trajectory of such particle satisfies the equation

$$\begin{aligned} \frac{dX}{dt}(x, t_{n+1}; t) &= \mathbf{u}(X(x, t_{n+1}; t), t) \\ X(x, t_{n+1}; t_{n+1}) &= x \end{aligned} \tag{6}$$

Note that  $X(x, t_{n+1}; t)$  is the point at time  $t$  corresponding to the characteristic curve of the operator  $\frac{\partial}{\partial t} + \mathbf{u} \cdot \nabla$ . Assuming that  $\mathbf{u}(\cdot, t)$  satisfies the conditions for the existence of a unique solution of (6) for all time  $t$ , see (C. Foias and Temam, 1985), we have that for  $t_n \leq t < t_{n+1}$

$$X(x, t_{n+1}; t_n) = x - \int_{t_n}^{t_{n+1}} \mathbf{u}(X(x, t_{n+1}; t), t) dt \tag{7}$$

It can be shown, see for instance (Suli, 1988), that (7) defines a continuous transformation of  $\bar{\Omega}$  onto itself provided that homogeneous Dirichlet boundary conditions for the velocity are used. For any  $(x, t) \in \bar{\Omega} \times [t_n, t_{n+1}]$ , we then integrate (1) along the characteristics to obtain

$$\begin{aligned} \mathbf{u}(x, t_{n+1}) &= \mathbf{u}(X(x, t_{n+1}; t_n), t_n) + \nu \int_{t_n}^{t_{n+1}} \Delta \mathbf{u}(X(x, t_{n+1}; t), t) dt - \\ &- \int_{t_n}^{t_{n+1}} \nabla p(X(x, t_{n+1}; t), t) dt + \int_{t_n}^{t_{n+1}} \mathbf{f}(X(x, t_{n+1}; t), t) dt \end{aligned} \tag{8}$$

It is clear that the evaluation of the integrals in (8) has to be approximated by a quadrature rule. In so doing, we shall obtain a time-marching algorithm to approximate  $\mathbf{u}^{n+1}$  and  $p^{n+1}$ . A number of characteristic-Galerkin schemes have been proposed by various authors to integrate (8), see for instance (Pironneau, 1982; Suli, 1988; Huffenus and Khaletzky, 1984). Using the first order upper limit quadrature rule to integrate (8) yields the characteristic backward Euler scheme. Based on optimal error analysis by Bermejo (Bermejo, 1995), we propose in this work a scheme that is obtained by combining the trapezoidal rule for the viscous term integral with the upper limit rule for the pressure term integral. Thus, a characteristic Crank-Nicolson scheme for the velocity and a first order implicit scheme for pressure are obtained. Hence, we can formulate our time-marching scheme to integrate (1) – (5) as follows.

Given  $\mathbf{u}^0$ , for any  $x \in \bar{\Omega}$  and  $n = 0, 1, \dots, N$

(i) Evaluate

$$X(x, t_{n+1}; t_n) = x - \int_{t_n}^{t_{n+1}} \mathbf{u}(X(x, t_{n+1}; t), t) dt. \tag{9}$$

(ii) Compute the interpolation of the velocity  $\mathbf{u}^{*n}$  at the foot of the characteristics

$$\mathbf{u}^{*n} = \mathbf{u}^n(X(x, t_{n+1}; t_n)). \tag{10}$$

(iii) Solve

$$\mathbf{u}^{n+1} = \mathbf{u}^{*n} + \frac{\Delta t \nu}{2} [\Delta \mathbf{u}^{n+1} + \Delta \mathbf{u}^{*n}] - \Delta t \nabla p^{n+1} + \frac{\Delta t}{2} [\mathbf{f}^{n+1} + \mathbf{f}^n(X(x, t_{n+1}; t_n))], \tag{11}$$

$$\nabla \cdot \mathbf{u}^{n+1} = 0, \tag{12}$$

subject to

$$\mathbf{u}^0 = \mathbf{u}_0(x) \quad \text{in } \Omega, \quad (13)$$

$$\mathbf{u}^{n+1} = \mathbf{g}_1^{n+1} \quad \text{on } \Gamma_1, \quad (14)$$

$$-p^{n+1} \mathbf{n} + \nu \frac{\partial \mathbf{u}^{n+1}}{\partial n} = \mathbf{g}_2^{n+1} \quad \text{on } \Gamma_2. \quad (15)$$

Details on the evaluation of steps (i) and (ii) can be found in (Allievi and Bermejo, 2000). Explanation of the numerical evaluation of step (iii) can be found in (Dean and Glowinski, 1993; Gonzalez and Bermejo, 2005).

#### 4 IMS GEOMETRY AND ION/PARTICLE CLUSTER TRACKING

We wish to compute the convection of an ion/particle cluster by a flow of air past a backward-facing-step-like geometry that mimics the longitudinal mid-section of the micro-scale chamber of a Ion Mobility Spectrometer (IMS). See Figure 3 for the geometrical setting of our model problem. The top and bottom boundaries are solid walls where non-slip boundary conditions are imposed. For the inflow a parabolic horizontal velocity profile is considered as  $(u, v) = (4(0.5 - y)(0.5 + y), 0)$ . Finally, for the outflow and for the detection outlets natural boundary conditions (NBC) are used. Air velocities are considerably smaller than the sound speed, hence the incompressibility assumption is duly satisfied.

The cluster of ion/particles is generated as a pulse at the inlet of the IMS device once the flow has reached a steady state. In order to measure its evolution in time, a pure homogeneous transport equation for the ions/particles concentration  $c$  is solved. Then

$$\frac{Dc}{Dt} = \frac{\partial c}{\partial t} + \mathbf{u} \cdot \nabla c = 0, \quad \text{in } \Omega \times [t_c, T] \quad (16)$$

subject to the initial conditions

$$c(\mathbf{x}, t_c) = c_0(\mathbf{x}) \quad \text{in } \Omega, \quad (17)$$

where  $c_0(\mathbf{x})$  is a prescribed distribution of ions/particles at a certain time  $t_c$ . In this work, a pulse is generated at  $t_c = 750T$  with value  $c_0 = 1$  at the inlet nodes and  $c_0 = 0$  elsewhere in the domain. This concentration of ions/particles is convected with the steady-state flow field computed from the solution of (1)-(2). In view of (16), we can write

$$c(\mathbf{x}, t^{n+1}) = c(X, t^n) = c(X(x, t_{n+1}; t), t) = \sum_{i=0}^n c_i^{t^n} \phi_n(X_i) \quad \text{in } \Omega \quad (18)$$

where  $\phi_n(X_i)$  are the basis functions evaluated at the foot of the characteristics (in general not at nodal locations) and  $c_i^{t^n}$  are the nodal values of the ions/particles cluster corresponding to the element hosting the foot of the characteristics curve.

#### 5 RESULTS

The equations in the problem described by (1)-(5) are re-written in non-dimensional form. Results using  $L = 100 \times 10^{-6}m$  as characteristic length,  $U = 10m/s$  as characteristic velocity and  $\nu = 10^{-5}m^2/s$  as the kinematic air viscosity. According to this scales the Reynolds number obtained is  $Re = 100$  and the characteristic time scale is  $T = L/U = 10^{-5}s$ .

The mesh used is made by Taylor-Hood triangular elements that contain six velocity nodes and three pressure nodes. It contains 42051 quadratic nodes and 20394 elements. The mesh size  $h = 0.1$  was uniformly assigned for the hole domain, with the only exception of the boundary lines that represent the detection electrodes where mesh size was locally reduced to  $h_o = 0.05$ .

To model the presence of detection electrodes, holes were introduced at the bottom part of the geometry downstream from the step. To evaluate the electrostatic attraction required by the actual electrodes of an IMS device, outflow boundary conditions were imposed on these holes. As a result, three different geometries were used in the computations: the first with no holes, and the second and third with three and five holes of  $a = 0.5$  units, Figure 3. Steady state flow conditions were reached at around  $t = 500T$  in all three cases. Prevailing tendencies of certain ions/particles to be attracted by the presence of the holes and other generalities of the flow are discussed in the remaining of this section.

Figure 4 shows streamlines for no holes, 3 and 5 holes. For all three configurations, the development of the typical stretched vortex occurs behind the backward-facing step. There is no appreciable evidence of changes in the shape of this recirculation zone between the geometries with holes and that when no holes are present. However, the effect on the streamlines is remarkable. The periodic attraction caused by the holes is clearly seen, the period roughly given by the separation between holes. Ions/particles traveling with the bottom half flow of the inlet channel are progressively attracted towards the holes. As expected, the effect of the attraction extends higher than half the flow of the inlet channel when the number of holes is increased from 3 to 5.

	0 hole	3 holes	5 holes
$\Delta p$	229.6339	193.9444	187.8998

Table 1: Pressure difference (Pa) between inflow and outflow boundaries at  $t = 500T$  seconds.

	3 holes	5 holes
First	-0.3983	-0.2883
Second	-0.3305	-0.2745
Third	-0.2475	-0.2547
Forth	-	-0.2339
Fifth	-	-0.2131

Table 2: Maximum vertical velocity at different holes for each geometry at  $t = 500T$  seconds.

	3 holes	5 holes
First	$8.7022 \times 10^{-5}$	$3.0922 \times 10^{-5}$
Second	$5.2571 \times 10^{-5}$	$2.6545 \times 10^{-5}$
Third	$2.4005 \times 10^{-5}$	$2.2380 \times 10^{-5}$
Forth	-	$1.8950 \times 10^{-5}$
Fifth	-	$1.5834 \times 10^{-5}$

Table 3: Flux of kinetic energy ( $J/s$ ) through the holes geometries at  $t = 500T$  seconds.

Figures 5 and 6 show contour plot for horizontal and vertical velocity components  $u, v$ . While the horizontal component of the velocity  $u$  is not qualitatively changed by the presence

	3 holes	5 holes
First	3.1972e-6	2.73884e-006
Second	1.1194e-5	5.7566e-009
Third	1.2409e-4	2.70734e-010
Forth	-	1.52111e-010
Fifth	-	3.47628e-005

Table 4: Maximum ion concentration at the different holes for the different geometries at  $t = 850T$  seconds.

of the holes, it is clear that the vertical component  $v$  is drastically changed when the holes are introduced in the geometry. Pressure contours for this velocity field are given in Figure 7. They correspond to the  $\Delta p$  values given in Table 1.

Table 2, the maximum values of the vertical velocity components at the holes have been compared for the different geometries studied. They are significantly higher than the horizontal ones at the boundaries that represent the holes. Therefore, the vertical velocity component is a good representation of the energy outflow. Table 3 shows kinetic energy flux through the holes obtained by integrating velocity profiles of Figure 8. Contrary to intuition, these results indicate that greater attraction efficiency is obtained when only 3 holes are used.

Figures 9 shows concentration contours of ions/particles being captured as the ion/particles cluster moves along the geometry with 5 holes. The figures correspond to  $T = 790$  ( $x_p=15.32$ ),  $T = 800$  ( $x_p=18.725$ ) and  $T = 810$  ( $x_p=21.385$ ), where  $x_p$  is the location of the concentration peaks measured from the step. The reduction in the peaks of ion/particles concentration clearly indicates that an important amount is being attracted by the holes. Peaks of concentration at  $t = 850T$  are given in Table 4, indicating that most of the ions/particles have evacuated the chamber in about 100 non-dimensional time units, the equivalent of 10 *msec*.

## 6 CONCLUSIONS

A Finite Element algorithm for the solution of the incompressible Navier-Stokes equations based on the Modified Method of Characteristics was implemented to simulate the advection of a cluster of ions/particles along a backward-facing-step-like geometry that mimics the longitudinal mid-section of the microscale chamber of an Ion Mobility Spectrometer (IMS). The attraction caused by the detection electrodes of an IMS device was simulated by means of out-flow boundary conditions that provided estimates of the energy necessary to attract the cluster. Contrary to intuition, a 3 hole configuration seems to be more efficient than its 5-hole alternative. As a result of this finding, we speculate that, when end electrodes are located a fixed distance apart, fewer electrodes would be recommendable.

## REFERENCES

- Allievi A. and Bermejo R. Finite element modified method of characteristics for the Navier-Stokes equations. *International Journal for Numerical Methods in Fluids*, 32(4):439–463, 2000.
- Bermejo R. A Galerkin-characteristic algorithm for transport-diffusion equations. *SIAM Journal of Numerical Analysis*, 32:425, 1995.
- Buryakov I., Krylov E., Nazarov E., and Rasulev U. A new method of separation of multi-atomic ions by mobility at atmospheric pressure using a high-frequency amplitude-asymmetric strong electric field. *International Journal of Mass Spectrometry and Ion Processes*, 128:143–148, 1993.

- C. Foias C.G. and Temam R. Lagrangian representation of the flow. *Journal of Differential Equations*, 57:440–449, 1985.
- Cumeras R., Gracias I., Figueras E., Fonseca L. Santander J., Salleras M., Calaza C., Sabaté N., and Cané C. Finite-element analysis of a miniaturized ion mobility spectrometer for security applications. *Sensors and Actuators B*, doi:10.1016/j.snb.2010.11.047, 2010.
- Cumeras R., Gracias I., Figueras E., Fonseca L. Santander J., Salleras M., Calaza C., Sabaté N., and Cané C. Planar micro ion mobility spectrometer modelling for explosives detection. In *8th Spanish Conference on Electron Devices, CDE2011*. 2011.
- Cumeras R., Gracias I., Ivanov P., Sabaté N., and Cané C. COMSOL simulation of acetone ions in planar ion mobility spectrometer. In *2009 Spanish Conference on Electron Devices*, pages 323–326. 2009.
- Dean E. and Glowinski R. *On some finite element methods for the numerical simulation of incompressible viscous flow*. In *Incompressible Computational Fluid Mechanics*, volume I. Cambridge University Press, 1993.
- Ewing R., Atkinson D., Eiceman G., and Ewing G. A critical review of ion mobility spectrometry for the detection of explosives and explosive-related compounds. *Talanta*, 54:515–529, 2001.
- Gonzalez L. and Bermejo R. A semi-Lagrangian level set method for incompressible Navier–Stokes equations with free surface. *International Journal for Numerical Methods in Fluids*, 49:1111–1146, 2005.
- Gresho P. Some current CFD issues relevant to the incompressible Navier–Stokes equations. *Computer Methods in Applied Mechanics and Engineering*, 87:201–252, 1991.
- Guevremont R. High-field asymmetric waveform ion mobility spectrometry (FAIMS). *Canadian Journal of Analytical Sciences and Spectroscopy*, 49(3):105–113, 2004.
- Guevremont R. and Kolakowski B. Using FAIMS to increase selectivity for LC-MS analyses. *American Laboratory*, 37(11):11–14, 2005.
- Guevremont R. and Purves R. Atmospheric pressure ion focusing in a high-field asymmetric waveform ion mobility spectrometer. *Review of Scientific Instruments*, 70(2):1370–1383, 1999.
- Heywood J. The Navier-Stokes equations: on the existence, regularity and decay of solutions. *Indiana University Mathematical Journal*, 29:639–681, 1980.
- Huffenus J. and Khaletzky D. A finite element method to solve the Navier-Stokes equations using the method of characteristics. *International Journal for Numerical Methods in Fluids*, 4:247–269, 1984.
- Iceman G. and Karpas Z. *Ion Mobility Spectrometry*. CRC Press, 1993.
- Iceman G. and Karpas Z. *Ion Mobility Spectrometry*. Taylor & Francis, 2005.
- Kalms A., Salleras M., Liu Z., Korvink J., Goebel J., Muller G., Smitier J., and Marco S. Numerical simulation of ion drift within ion mobility spectrometers in high pecelet conditions using FEM techniques. In *13th International Conference on Thermal, Mechanical and Multi-Physics Simulation and Experiments in Microelectronics and Microsystems*. 2007.
- Ladyzhenskaya O. *The mathematical theory of viscous incompressible flow*. Gordon & Beach, 1969.
- Miller R., Eiceman E., Nazarov E., and King A. A novel micromachined high-field asymmetric waveform-ion mobility spectrometer. *Sensors and Actuators B*, 67:300–306, 2000.
- Miller R., Nazarov E., Eiceman E., and King A. A MEMS radio-frequency ion mobility spectrometer for chemical vapor deposition. *Sensors and Actuators A*, 91(3):301–312, 2001.
- Ortiz J., Allievi A., Lamagna A., and Boselli A. Electro-aerodynamic microflow simulation in

- a MEMS-based ion mobility spectrometer. In *18th Annual Conference of the International Society for Ion Mobility Spectrometry*. 2009.
- Owlstone Nanotech Inc. White paper. In [www.owlstonenanotech.com](http://www.owlstonenanotech.com). 2006.
- Pironneau O. On the transport-diffusion algorithm and its applications to the Navier-Stokes equations. *Numerische Mathematik*, 38:309–322, 1982.
- Smolarkiewicz P. and Pudykiewicz J. A class of semi-Lagrangian approximations for fluids. *Journal of Atmospheric Sciences*, 49:2082–2096, 1992.
- Staniforth A. and Cote J. Semi-Lagrangian schemes for atmospheric models a review. *Monthly Weather Review*, 119:2206–2223, 1981.
- Strain J. Semi-lagrangian methods for level set equations. *Journal of Computational Physics*, 151:498–533, 1999.
- Suli E. Convergence and nonlinear stability of the Lagrange-Galerkin method for the Navier-Stokes equations. *Numerische Mathematik*, 53:459–483, 1988.
- Teepe M., Baumbach J., Neyer A., Schmidt H., and Pilzecker P. Miniaturized ion mobility spectrometer. *International Journal of Ion Mobility Spectrometry*, 4(1):60–64, 2001.
- Temam R. *Navier-Stokes equations: theory and numerical analysis*. North-Holland, 1985.
- Xu J., Whitten W., and Ramsey J. Space charge effects on resolution in a miniature ion mobility spectrometers. *Analytical Chemistry*, 72:5787–5791, 2000.
- Zimmermann S. and Barth S. A miniaturized ion mobility spectrometer for detection of hazardous compounds in air. In *14th International Conference on Solid-State Sensors, Actuators and Microsystems*, pages 1501–1504. 2007.

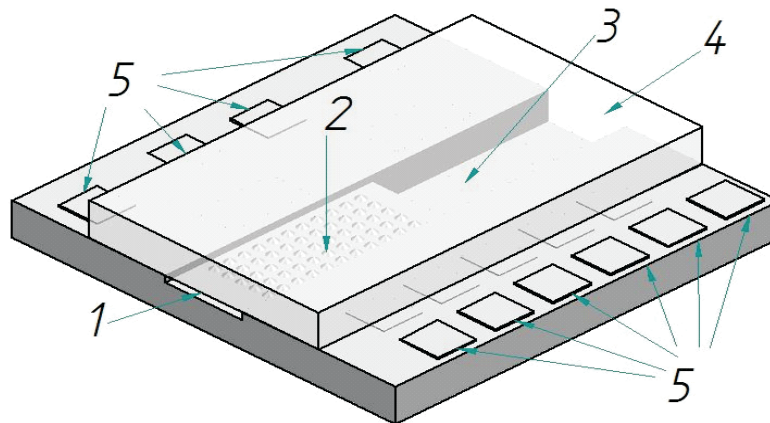


Figure 1: Microdevice for ion mobility spectrometry showing the chamber/drift tube. 1. Inlet, 2. ionization region, 3. detection region, 4. outlet, 5. contact pads

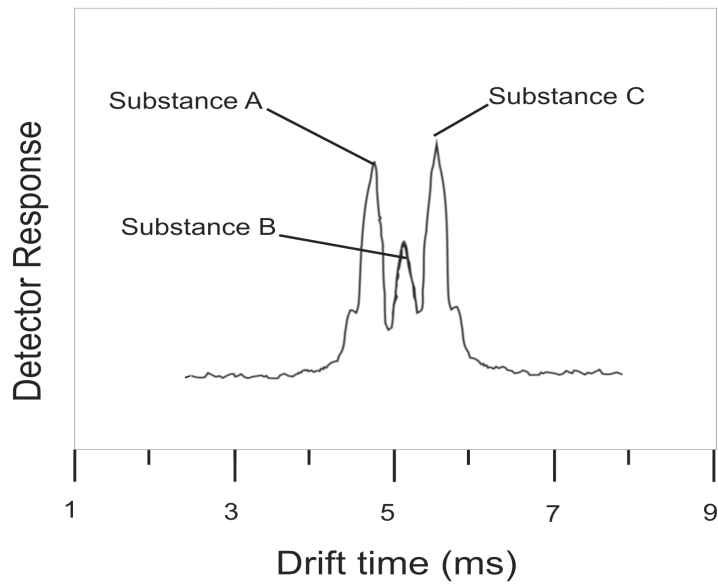


Figure 2: Typical histogram for an Ion Mobility Spectrometry (IMS).

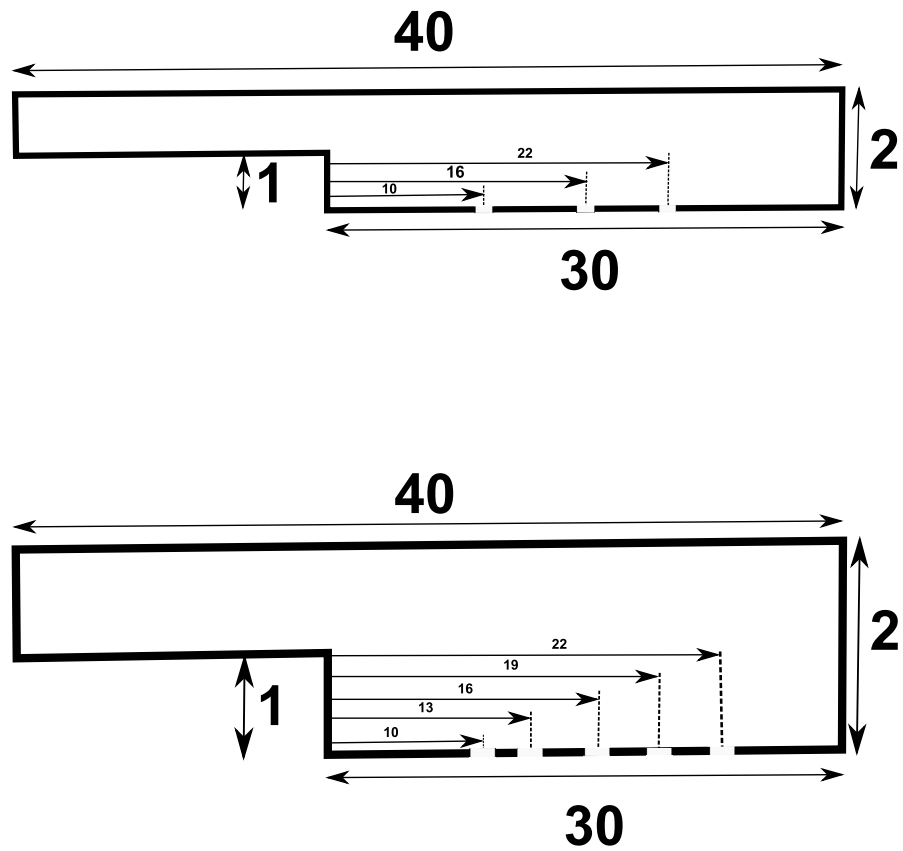


Figure 3: General geometry for 3 (top) and 5 (bottom) holes.

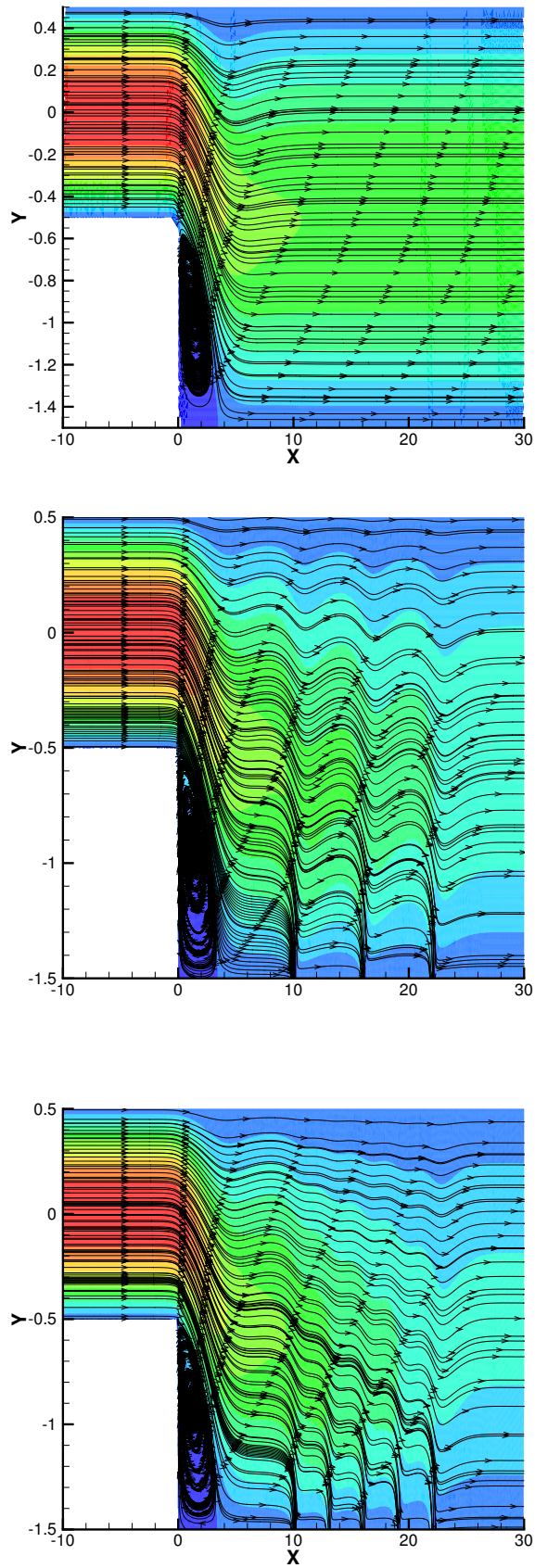


Figure 4: Streamlines at  $t = 500T$  seconds. Top: no holes, middle: 3 holes and bottom: 5 holes.

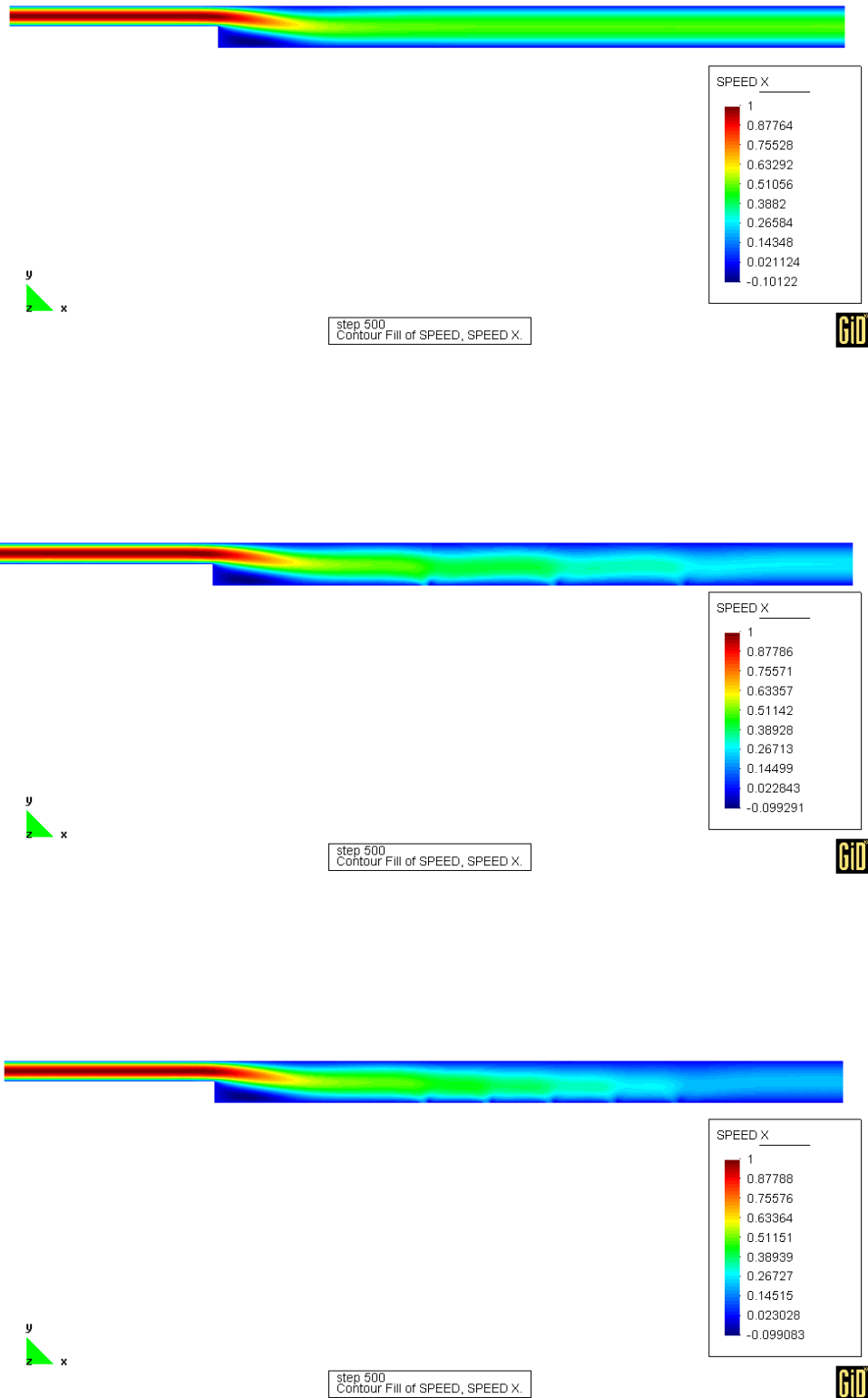


Figure 5: Horizontal velocity component  $u$  for the different configurations at  $t = 500T$  seconds. Top: no holes, middle: 3 holes and bottom: 5 holes

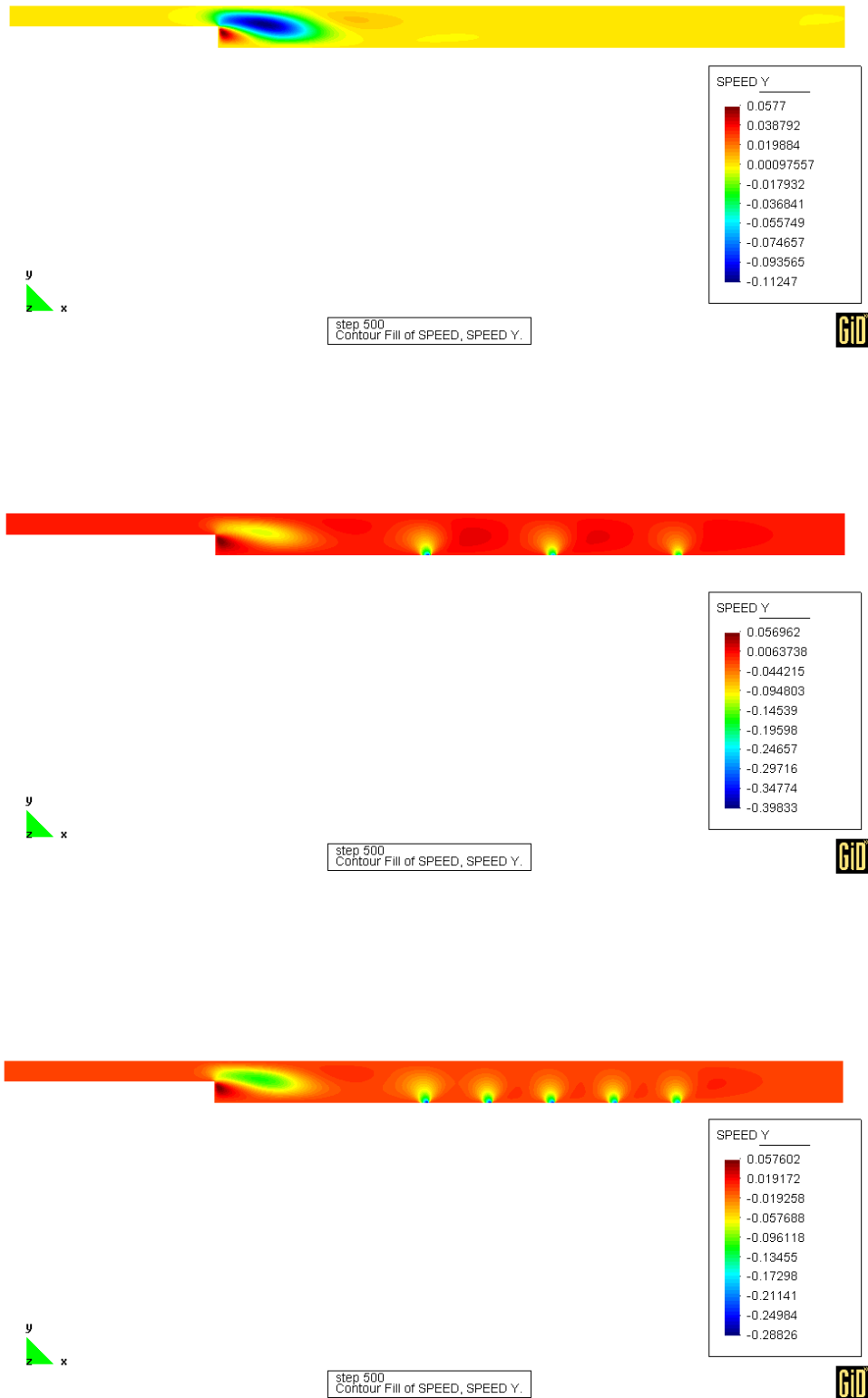


Figure 6: Vertical velocity component  $v$  for the different configurations at  $t = 500T$  seconds. Top: no holes, middle: 3 holes and bottom: 5 holes

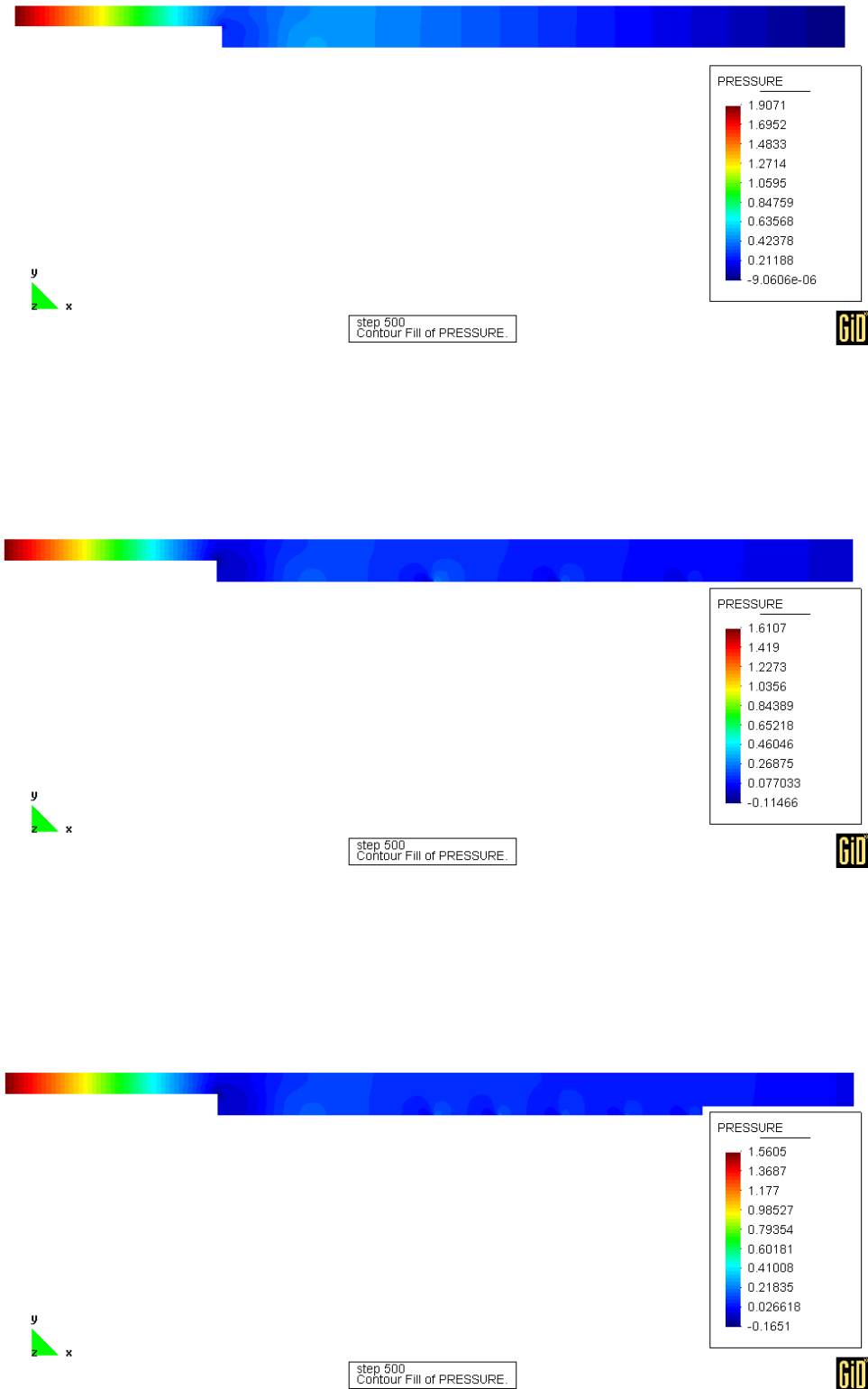


Figure 7: Pressure for the different configurations at  $t = 500T$  seconds. Top: no holes, middle: 3 holes and bottom: 5 holes

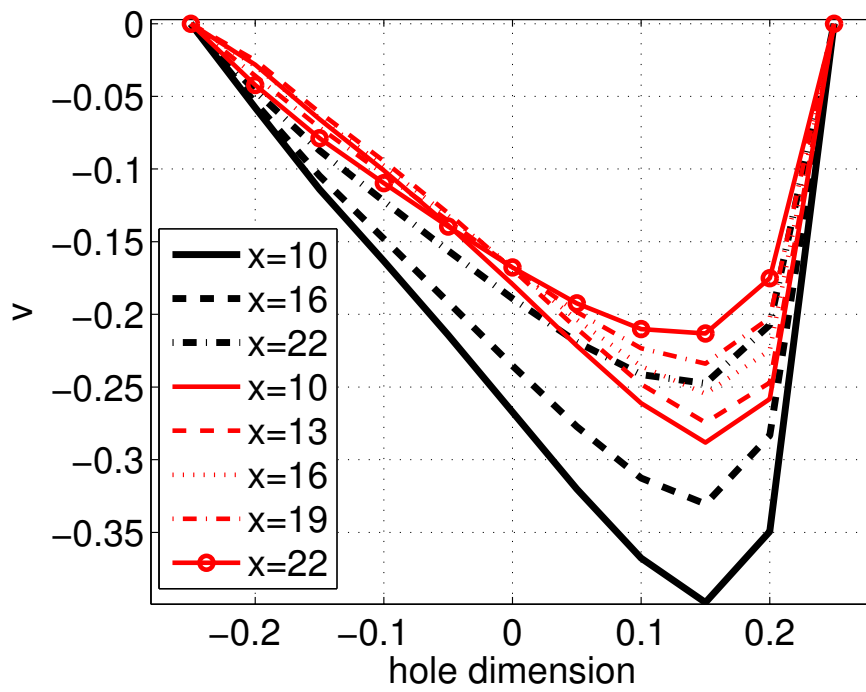


Figure 8: Vertical velocity profiles at  $t = 500T$  seconds along the holes for the different configurations.

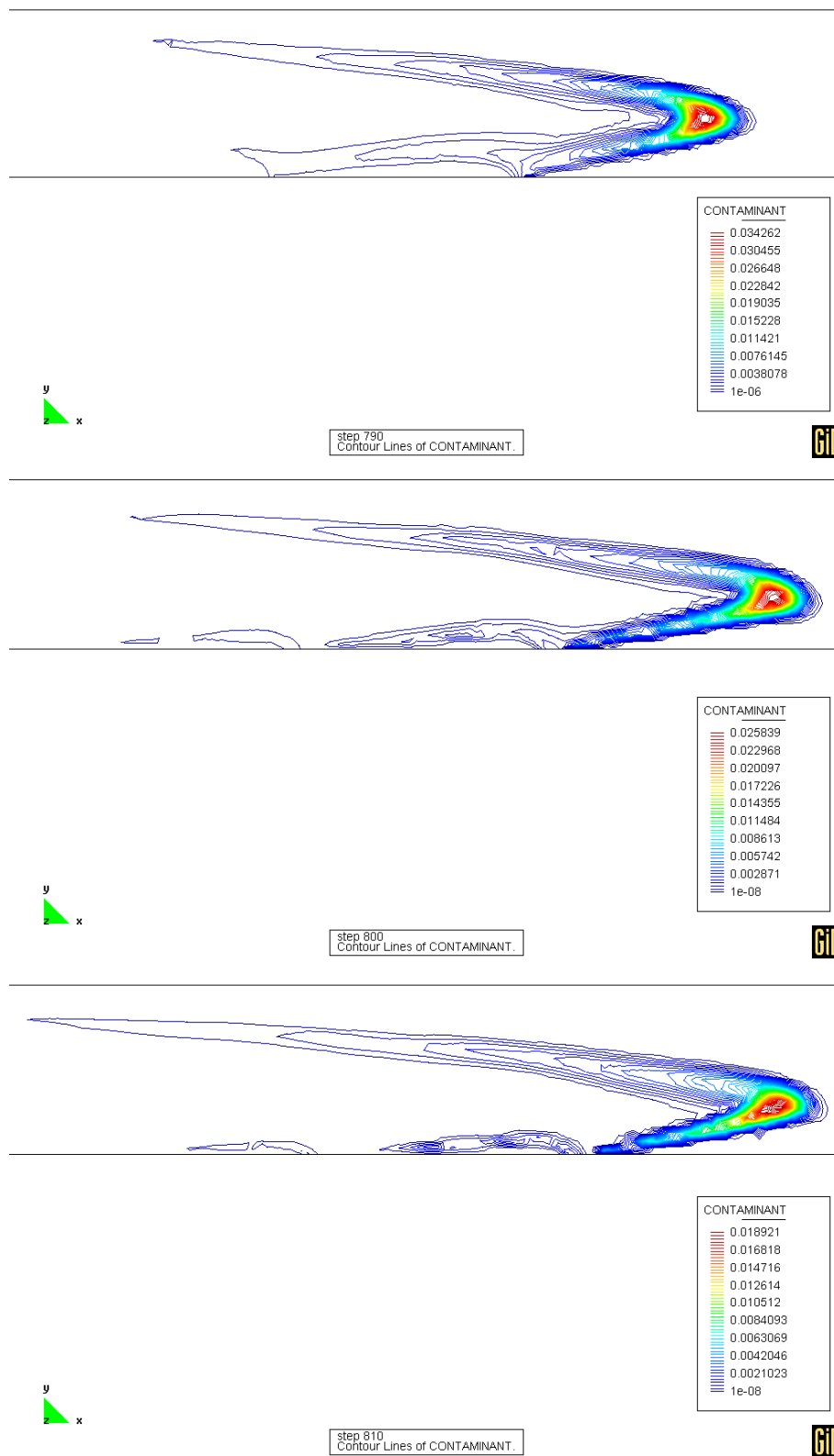


Figure 9: Ion concentration, 5-hole geometry.  $T = 790$  ( $x_p=15.32$ ),  $T = 800$  ( $x_p=18.725$ ) and  $T = 810$  ( $x_p=21.385$ ).